Abraldes P., Cabaleiro M., Sousa H.S., Branco J.M. (2022). Use of polar coordinates for improving the measurement of resistant cross-sections of existing timber elements combining laser scanner and drilling resistance tests. Measurement 204(112027). pp 1-13 (doi.org/10.1016/j.measurement.2022.112027)

Pre-print version. The final publication is available at sciencedirect.com: http://doi.org/10.1016/j.measurement.2022.112027

Use of polar coordinates for improving the measurement of resistant cross-sections of existing timber elements combining laser scanner and drilling resistance tests

ABSTRACT

Historic timber structures typically have elements with irregular cross-sections often with decayed segments, making of extreme importance to have proper methods to obtain the resistant cross-section. Knowing as accurately as possible the measurements of the resistant section of these beams is fundamental for the structural safety analysis. Small changes on the size and geometry of the resistant cross-section may be fundamental in an intervention decision process. In this work an algorithm was created that allows to obtain the geometry of the resistant section of existing timber beams by use of data obtained by laser scanning of the external apparent sections combined with drilling resistance tests. The algorithm is based on polar coordinates and proved to obtain more reliable resistant cross-sections than those obtained solely by common practice using drilling resistant tests. The developed algorithm was calibrated with a laboratory beam and subsequently applied and validated in a case study.

Keywords: Decayed timber, cloud of points, resistant cross-section, drilling resistance tests.

1. INTRODUCTION

Wood is a natural material used in structures of all kinds. Due to that, the condition state of these buildings must be analysed periodically due to a large number of factors that can influence the development of decay, such as changes in water content or biotic agents (e.g. xylophage insects and fungi). Regarding the elements scale, that decay will often progress from the exterior to the interior of the cross-section destroying layer after layer. Accounting to that progressive decay it would be important, for a reliable safety assessment, to be able to calculate the geometry of the resistant area taking into account the exterior shape of the elements.

The irregular shape, that timber beams from existing old structures usually present, makes it very complex to manually determine the dimensions of the apparent sections. Currently, techniques such as laser scanning is being successfully used to obtain these measurements and subsequent 3D modelling of historic buildings and structures, not only made of timber but also with other materials [1-3]. In several works, the 3D models created from laser scanning were after used for finite element modelling and subsequent structural analysis [4-8]. In this case, laser scanning is one of the most suitable methods to automatically obtain the apparent shape of irregular beams, through which a three-dimensional point cloud of the studied beam is generated [8-10]. Different methodologies, such as seen in Cabaleiro et al.[8], can be used to obtain the shape of the apparent section of a beam. In Cabaleiro et al.[8], the point cloud of the beam is cut in each of the analysed sections and is projected to a plan in order to apply the Alpha Shape algorithm [11], which provides the apparent perimeter of the studied section. In many cases, one of the faces of the beam is not visible to the laser scanning impeding the reading by the laser scanner. In that cases, the proposed framework may resort to complementary methods combining different types of tests [10].

Historic timber buildings often present elements with different levels of decay. To evaluate this degree of decay, non-destructive tests (NDT) and semi-destructive tests (SDT) are usually carried out. Some of these tests are: visual inspection and photogrammetry [12], moisture content measurements [13], ultrasonic wave [14,15], ambient vibration tests [16], pin penetration tests [17] and drilling resistance tests. This last one allows to obtain information regarding the state of conservation of the interior of the timber element cross-section. Drilling resistance tests consists of an instrument similar to a drill with a bit of diameter between 1.5 mm and 3.0 mm that advances at a constant speed through the wood element, indicating the energy needed to maintain that movement. With this information, a graph is constructed, in which it can be determined the length of three intervals for elements with superficial decay: (i) decayed wood at the entry surface of the drilling resistance test, (ii) resistant wood and (iii) decayed wood at the exit surface of the test [18-22]. The number of drillings will depend on the dimensions of the analysed section, being more common two to four measurements. From the information of the drilling resistance graphs and knowing the position of the entry and exit points (which can be obtained from the point cloud) the resistant points are obtained. Current methods derive the resistant cross-section by connecting these points with straight lines and constructing polygon surface (Figure 1) [8,10]. However, when using this method, an error is being made due to the non-consideration of all the possible resistant section of the beam in the analysed section (Figure 1). This error will decrease as the number of measurements increases. In general, a smaller resistant cross-section than the real one will be calculated, which can lead to over conservative decisions related to the safety of the structure.

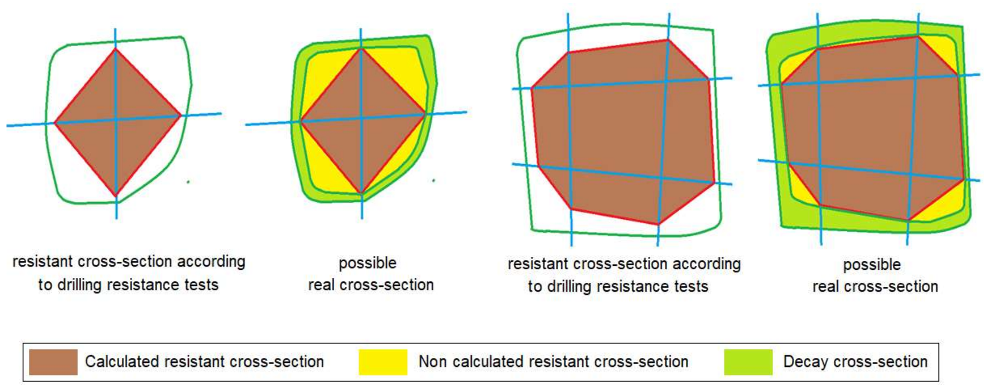

Figure 1. Example of differences between the resistant cross-section calculated with a polygon constructed using with the drilling resistance tests graphs and the real resistant cross-section of the element.

The main objective of this work is to develop an algorithm that, starting from the resistant points obtained with the drilling resistance tests and taking into account the real apparent external shape of the beam according to the laser scanning, provides more accurate resistant sections of the beam, than the current ones obtained only by making a polygon using the drilling resistance test data. The new calculated section, much closer to the real value, will be called "Improved Resistant Section". In addition, another objective to be achieved with this algorithm is that the calculation of this improved resistant section may be independent of the number of drillings, therefore allowing for the use of less measurements. Overall, a more accurate definition of the size and geometry of the resistant cross-section is a preponderant variable for a reliable decision making process when one must consider if to intervene and what type of intervention to be carried out.

To verify the developed algorithm, the framework will first be calibrated in laboratory test conditions, in which six drillings per cross-section of a beam will be made. Combining these drillings, the most common polygonal resistant surfaces: rhombus, hexagons, octagons and dodecagons will be constructed. Finally, the results obtained from the improved resistant sections calculated by the algorithm will be compared with the real resistant areas. Finally, the algorithm will be applied and validated in a case study in the Convent of Saint María Madalena of the Converted (Braga, Portugal). In this case study, the developed algorithm has also proven to be efficient when not having access to all the faces of the element, as the element is in direct contact with the room's ceiling.

2. THEORY - PROPOSED METHODOLOGY

With the objective of obtaining the improved resistant sections of the beams, the proposed methodology consists of the steps provided in Figure 2. Each step will be detailed in the following subsections.

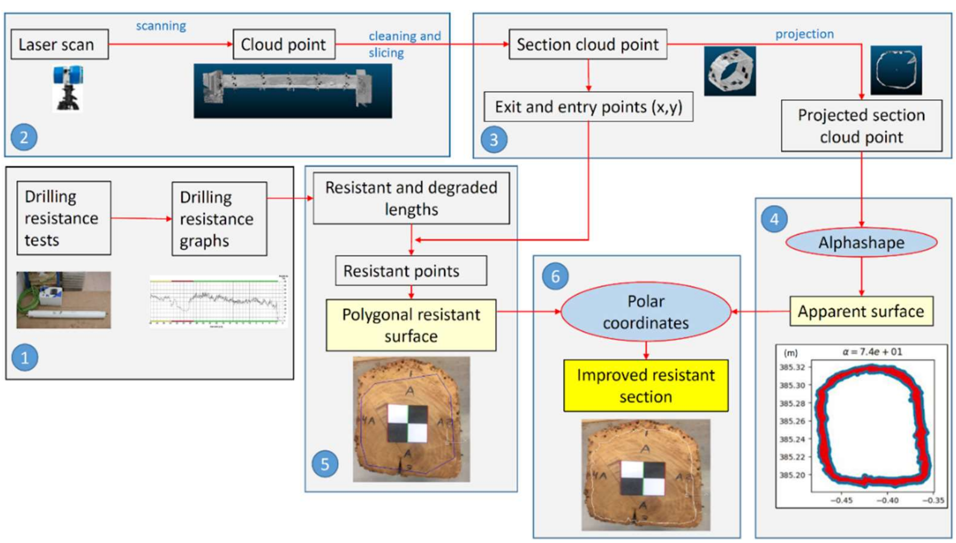

Figure 2. Outline of the proposed methodology: 1) Drilling resistance test testing, 2) Laser scanning of the beam, 3) Slicing and projection of the tested spans, 4) Calculation of the beams' apparent sections, 5) Polygonal resistant section calculation, 6) Improved resistant section calculation.

2.1. Drilling resistance tests

Four drillings are recommended to be considered in each of the beam cross-sections (two with vertical drills and two with horizontal drills). In each exit and entry points a target must be placed in order to find these points appropriately within the point cloud generated during the scanning process [10]. A section from each opposite side and a central section must be selected for the analysis in each beam. It is also recommendable to analyze all those parts where there are abrupt changes, or the section is considerably decayed. Drillings should be spaced at equal distances (i.e: a 1/3 distance from the outside edge, when considering two drillings per surface).

2.2. Laser scanning of the beam

Several scans are performed from different points so as to capture all the visible faces of the beam. Then, the multiple point clouds generated are recorded in a single point cloud [23]. Subsequently every item not belonging to the beam is removed for the purpose of obtaining a complete and clean point cloud.

2.3. Slicing and projection of the drilling resistance tests

The first action is to make a linear regression calculate the beam's longitudinal axis [24,25]. Then the point cloud is sliced for each of the drilled sections. The analyzed section must have the minimum thickness in order to collect all the targets (see Figure 3.a). Finally, an orthogonal projection of the cross-section is made to the beam's longitudinal axis.

2.4. Calculation of the beams' apparent section

As similarly carried out by Cabaleiro et al. [26], the Alpha-shape algorithm is applied in each section to calculate the apparent section. Then two lines are obtained: one interior and exterior. As in the work of Cabaleiro et al. [8], the interior one is chosen since it is free from possible external noise coming from the point cloud (Fig. 3).

2.5. Calculation of the polygonal resistant section

For the calculation of the polygonal resistant section the following data is considered: the entry Pr_e (Xe, Ye) and exit Pr_s (Xs, Ys) points of each drilling resistance test, obtained by the point cloud (Figure 3.a); and the information provided by the corresponding drilling resistance graph (Figura 3.c). Taking the coordinates of the entry Pr_e (Xe, Ye) and exit Pr_s

(Xs, Ys) points as a basis, the real length of the drilling resistance test L_w inside the beam is calculated following Equation 1:

$$L_w = \sqrt{(X_e - X_s)^2 + (Y_e - Y_s)^2} \qquad (1)$$

Following Equation 2 it is also possible to calculate the direction of the drilling:

$$y = \frac{Y_s - Y_e}{X_s - X_e}\, x + \left[Y_e - \left(\frac{Y_s - Y_e}{X_s - X_e}\right) X_e\right] \qquad (2)$$

Based on the drilling resistance test data, the length values of decayed timber at the entry (L_{de}) and resistant timber (L_r) are acquired. With the previous data and the total length of the L_w, following Equation 3, the value of the length of the decayed timber at exit (L_{ds}) is obtained (Figure 3.b):

$$L_{ds} = L_w - L_{de} - L_r \qquad (3)$$

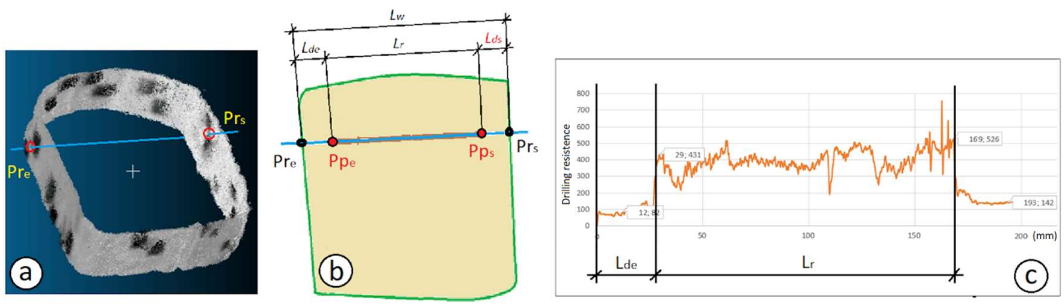

Figure 3. a) Drilling resistance test entry and exit points in the point cloud, b) Outline of the degraded and resistant length calculation in the section, c) Drilling resistance graph showing the degraded entry and resistant length.

The length value of decayed timber at the exit point cannot be attained straight from the test data, since during the testing process the drill bit comes out of the beam in a variable and unknown distance in each case. Figure 3.c provides an example of a drilling resistance graph indicating the entry points of the drill bit into the timber, the beginning of the resistant area, the end of the resistant area and the exit of the drill bit.

The coordinates of the drilling resistance test points are calculated taking the value of these lengths, the coordinates of the entry point and the direction of the test. The coordinates indicate the starting (Pp_e) and ending (Pp_s) point of the resistant cross-section.

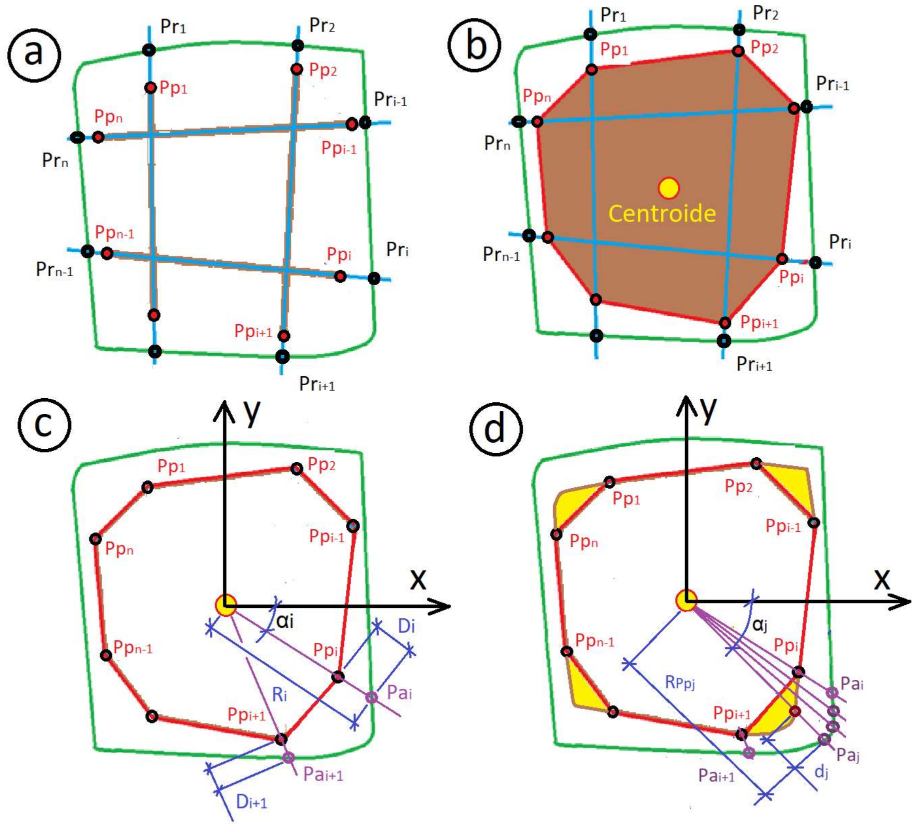

Figure 4. Outline of the optimized section calculation process.

This process is employed with every drilling resistance test used in each section (Figure 4.a). Having this data collected, one can continue to the construction of the polygon (octagon in case of 4 drillings). The polygonal resistant section of each cross-section (Figure 4.b) is defined by connecting the found points (Pp_i). The centroid (*Ce*) of the resistant polygon may also be calculated, as well as its area values and inertia moments regarding to the vertical and horizontal axis passing through the centroid.

2.6. Calculation of the improved resistant section

The next step is to calculate the coordinates of the intersection point Pa_i on the apparent exterior contour of the section originated by the straight line connecting the centroid (*Ce*) and the polygon point defined by the Pp_i drilling resistance tests (Figure 4.c). Then, the distance between each Pa_i point and its corresponding Pp_i points is calculated using Equation 4:

$$D_i = \sqrt{(X_{Pp_i} - X_{Pa_i})^2 + (Y_{Pp_i} - Y_{Pa_i})^2} \quad (4)$$

Equation 4 enables the calculation of the decay distance value *Di* in direction of the line connecting each Pp_i point with the centroid.

Next, Pp_i, Pa_i and all defining points of the beam's apparent section are converted from Cartesian coordinates (x, y) to polar coordinates (r, α), where *r* is the radius or modulus and *α* is the angle formed with de horizontal coordinate. The beginning of the coordinates is the centroid of the section. From this moment on, in order to calculate the improved resistant section, polar coordinates are used.

Firstly, the number of points (n_j) in each span of the apparent section between two P_{ai} and P_{ai+1} points are counted. Then, taking into account the value of decay D_i and D_{i+1}, belonging to the P_{ai} and P_{ai+1} points and for number of n_j points in each span, following Equation 5, the value of decay in each (n_j) point of the interval points (P_{ai} to P_{ai+1}) of the apparent section is calculated, so that the value varies progressively between consecutive points:

$$d_j = D_i + (D_{i+1} - D_i) * \frac{j}{n_j} \quad (5)$$

Following Equation 6, new coordinates are calculated for each of the points of the optimized resistant section by using the polar coordinates of each point from the apparent section:

$$Ro_j = \left(R_{Pp_j} - d_j\right), \alpha_j \qquad (6)$$

The new Ro_j radius value will be the remainder of the polar coordinate R_{Ppj} of the corresponding point minus the d_j value. The polar coordinate angle (α_j) will remain the same (Figure 4.d). The improved resistant section is obtained by connecting all these points.

Since using the algorithm the apparent section can be attained on the basis of laser scanning data, and employing the optimized resistant section values, one can calculate the decay percentage of the beam. Equation 7 calculates the degree of decayed area in each section:

$$\%_{Decay} = \frac{A_{apparent} - A_{optimized\ resistant}}{A_{Apparent}} * 100 \qquad (7)$$

2.7. Closing of open sections

For beams that, after the scanning, do not provide information about one of the faces in the point cloud, the section will be closed following the procedure detailed in Cabaleiro et al. [10]. This is a common situation in roof and floor beams where the face in contact with other elements is not visible. Before applying the Alpha Shape algorithm, the projected point cloud of the section must be closed. Vertical drillings will be considered perfectly vertical. The point defining the closing line (Ppv_i) of the section will be the point where the drilling resistance test stops showing resistant area (Figure 5.a). In order to avoid problems with possible atypical values due to noise, a SOR (Statistical Outlier Removal) filter is applied first to the projected section for the purpose of eliminating atypical values of the cross-section point cloud.

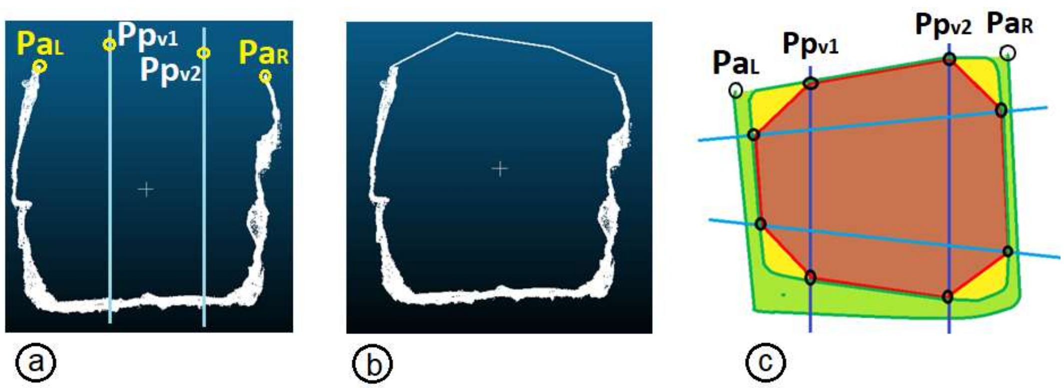

Figure 5. Outline of the point cloud section closing. a) Calculation of drilling resistance test vertical end P_{pvi} points and calculation of apparent open section end P_{aL} and P_{aR} points, b) Apparent section closing, c) Improved resistant section.

As done in Cabaleiro et al [10], the upper right extreme point (P_{aR}) and upper left extreme point (P_{aL}) of the point cloud is calculated. Finally, as a means to obtain the closing of the open section (Figure 5.b), P_{aL} is connected to P_{pv1}, P_{pv1} with P_{pv2} and P_{ar}. Hereafter, the previous steps shall be applied in order to calculate de improved resistant section (Figure 5.c).

3. CALCULATION - LABORATORY CASE STUDY

3.1. Employed methodology

As to verify the proposed methodology and algorithm, an element was studied in laboratory conditions. The following steps were considered: a) drilling resistance tests; b) beam laser scanning; c) cut and projection of the drilling resistance test sections; d) calculation of the beam apparent surface; e) calculation of the polygonal resistant section; f) calculation of the improved resistant section; g) calculation of the real resistant section; h) comparison and analysis of the results.

3.2. Drilling resistance tests

Usually two drillings are made for small-section beams, specifically one vertical and one horizontal, both in the middle of their corresponding face. This provides a resistant rhombus-shaped resistant polygon (Figure 6.a). When a small section has one larger side, it is also common to make two drillings there and one drilling in the narrow side. A total of three drillings are made and a hexagon is formed (Figure 6.b-6.c). It is worth stressing that making two drillings in large sections in order to save time is also common practice. Therefore, it is particularly important to verify the operation of the algorithm in two-drilling cases. Hence, one of the objectives of the laboratory testing is to compare the algorithm results when the number of drillings varies (Figure 6).

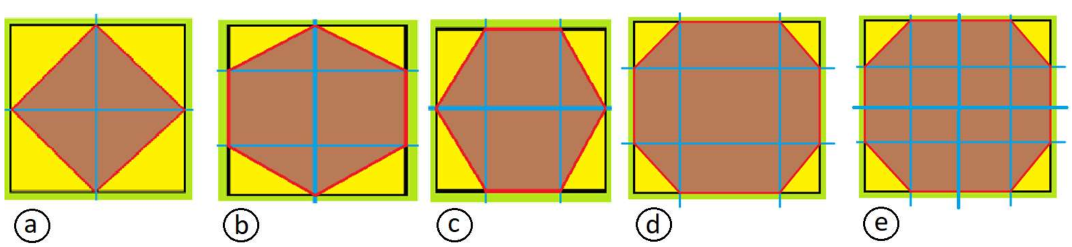

Figure 6. Different combinations depending on the number of drilling resistance tests made. a) Two-drilling rhomb, b) Vertical hexagon with three drillings, c) Horizontal hexagon with three drillings, d) four-drilling octagon, e) six-drilling dodecagon.

For the laboratory testing, two segments with 1 m length from an irregular-section timber beam were cut. More specifically, it was a beam with approximately 110x125 mm^2 cross-section made of chestnut (*Castanea sativa* Mill) (Figure 7.a). A total of six drillings were made in each of the four studied ends (three horizontal and three vertical). The tests were performed with a 3450-S Resistograph from RINNTECH. Targets were placed in the entry and exit points of the drilling resistance test drillings, which allowed an easier identification of those points in the point cloud. Once the drilling resistance testing was done, the laser scanning of the beams was carried out from 8 different positions using a FOCUS 3D X 130-HDR laser scanner from FARO. In this way it was possible to register the point cloud of both beams (Figure 7.b).

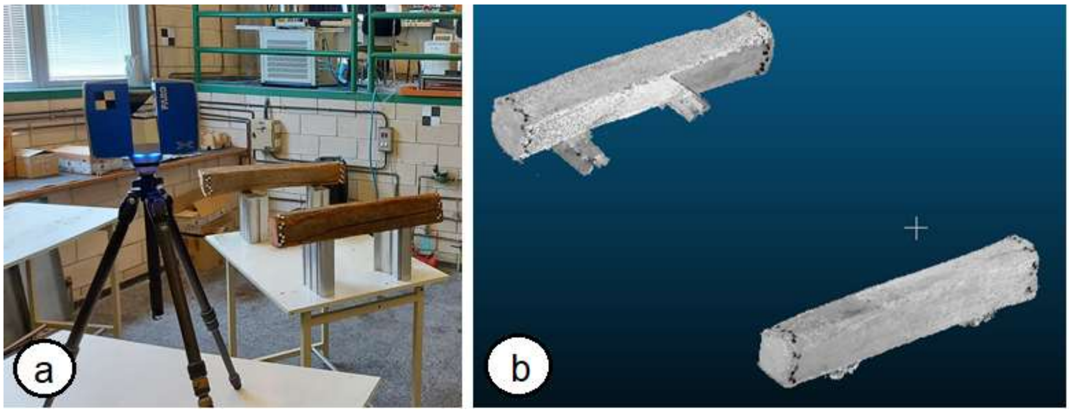

Figure 7. a) Beam scan in the laboratory, b) Complete cloud point of both beams.

The initial point clouds had approximately 170 million points, while the point cloud of the beam resulting from the cleaning and connecting the previous point clouds had approximately 20 million points.

As of the six drillings performed and the laser scanning, the results achieved by the algorithm could be analyzed in each case: a dodecagon (six drillings), an octagon (four drillings), two hexagons (three drillings) and a rhomb (two drillings). Finally, by cutting each section, using photogrammetry with a known scale board and considering an automated drawing software, the real apparent section and real resistant section were obtained.

3.3. Results and discussion

The graph of Figure 8 shows the average error made by traditional methods (polygonal resistant section) and the algorithm (improved resistant section) in each of the studied cases. For that purpose, the results obtained from both methods were compared with the real values of the resistant section attained by slicing the beams.

Results show how the error caused by employing a resistant polygon decreases as the number of drillings increase. It is worth highlighting the results obtained for the rhomb configuration (use of only two drillings) as it is the most employed technique for the analysis of beams of small section. The average area error committed by the polygonal resistant section exceeds 46.7%, while average errors in inertia moments reach 70.8%.

On the other hand, the improved resistant section calculated by the algorithm has an average area error less than 2.4% and an average error in inertia moments less than 4.6% in both cases (I_x and I_y). Therefore, results provided by the algorithm show an error reduction of 44.3% in area and of 166.2% in inertia calculation compared to the usual two-drilling case.

In the remaining cases improvements are also achieved, although at a smaller magnitude. The hexagon has an average area error made by the polygonal resistant section higher than 19.0%, while average errors in inertia moments are close to 34.9%. The improved resistance section calculated by the algorithm has an average area error lower than 2.2% and an average error in inertia moments lower than 4.7% in both cases (I_x and I_y). The octagon has an average area error made by the polygonal resistant section higher than 9.0%, while average errors in inertia moments are close to 18.2%. The improved resistance section calculated by the algorithm has an average area error of 2.6% and an average error in inertia moments lower than 6.5% in both cases (I_x and I_y).

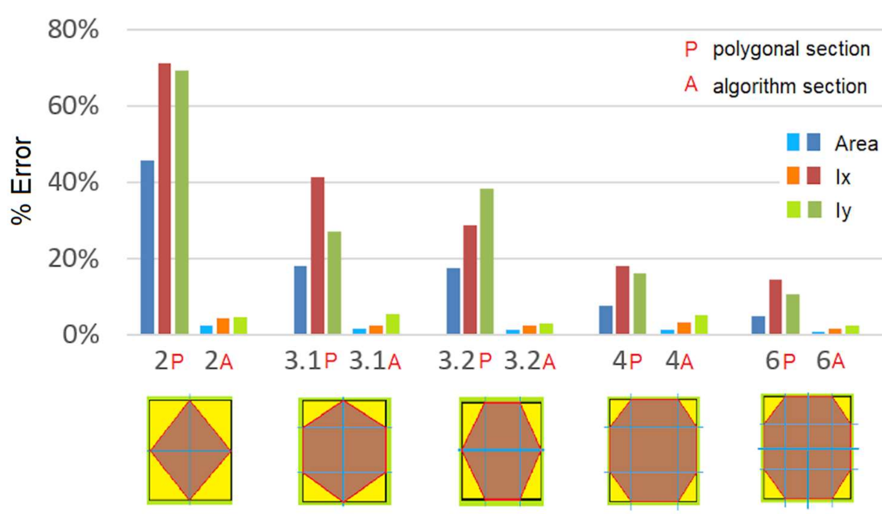

Figure 8. Errors made in the real resistant section for each number and combination of drilling resistance tests, as well as for the calculation by traditional method of the resistant polygon.

In general, data obtained from the resistant section is on the safe side. That is, even though the value is lower than the real one, there was 8.3% of measurements that gave higher values than the real ones. The average committed error value did not exceed 2.7% in these cases and was not higher than 5.0% (maximum error: 4.9%) in any case.

Figure 9 shows a more detailed example of one of the sections, as well as its results in Table 1.

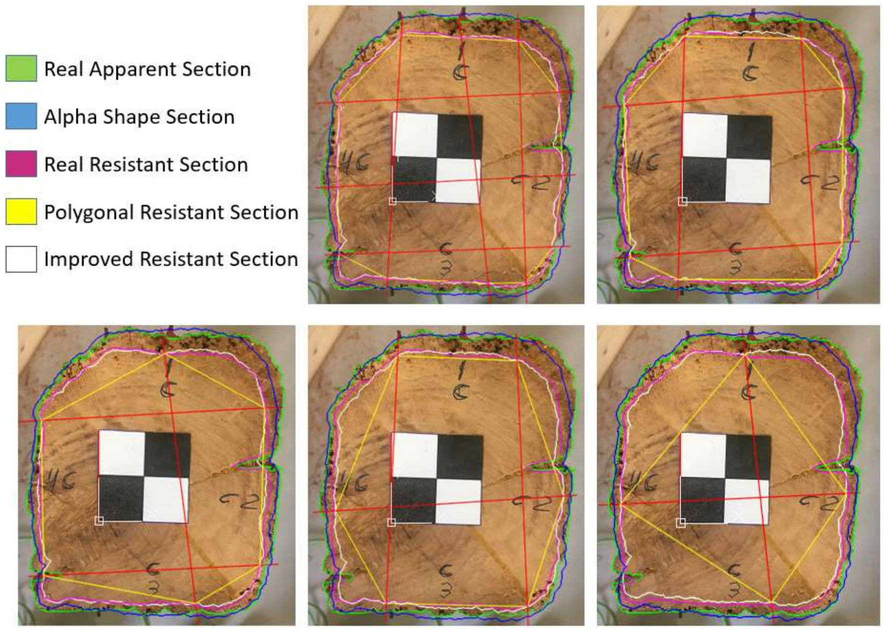

Figure 9. Detailed real, polygonal and improved resistant section, the real apparent and algorithm section. a) Dodecagon with six drillings, b) Octagon with four drillings, c) Horizontal hexagon with three drillings, d) Vertical hexagon with three drillings, e) Rhomb with two drillings.

Table 1. Data from one laboratory-tested section.

RESISTANT SECTION	**AREA (cm²)**	**I_X (cm4)**	**I_Y (cm4)**
REAL	103.5	976.0	784.0
RHOMB	56.2	289.7	246.4
ALGORITHM RHOMB	101.1	938.0	739.0
HEXAGON 1	87.5	625.0	613.7
ALGORITHM HEXAGON 1	103.0	973.0	767.6
HEXAGON 2	86.1	741.0	484.2
ALGORITHM HEXAGON 2	102.4	974.6	743.2
OCTAGON	97.9	867.9	691.9
ALGORITHM OCTAGON	103.4	989.0	763.6
DODECAGON	99.6	877.6	726.9
ALGORITHM DODECAGON	102.8	961.2	768.6

4. CALCULATION – ONSITE CASE STUDY

4.1. Description of the case study

The Convent of Saint María Madalena or of the Converted, in Braga, Portugal (Figure 10) was considered as case study. The building dates from the 18th century (inaugurated in 1772) and since them has served several purposes. It is a granite masonry building of baroque style (Figure 10.a). At present the building is partially abandoned. The current purpose is to carry out a recuperation process of the building, keeping as many elements from the original structure as possible, especially the main supporting beams. Figure 10.b shows pictures of the hall and the beam considered for this case study, which presents signs of severe decay.

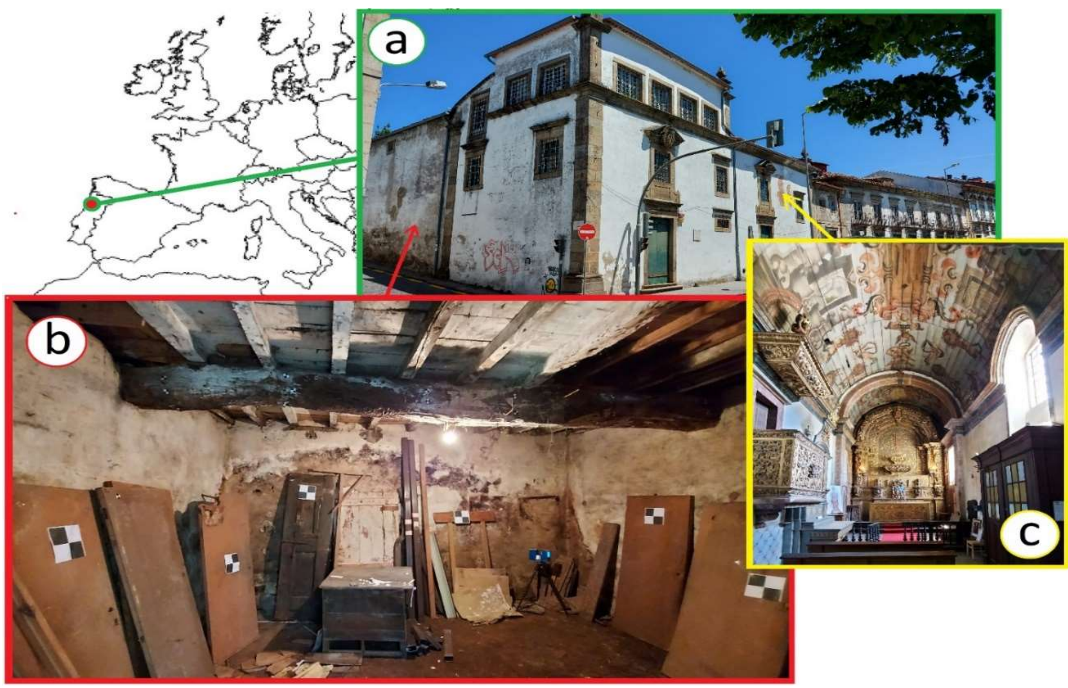

Figure 10.Convent location. a) facade, b) Hall to be restored in the case study, c) Santa María Madalena chapel.

The beam analyzed is supported by the two granite walls of the room. Its total length is 4.8 m with considerable irregular and variable section along its longitudinal axis.

4.2. Performed tests

The selection of the sections to be tested was based on the principle of characterizing the critical sections (sections with higher loads, namely mid-span and near the supports) and sections where higher level of decay and geometry irregularity was found. In this sense, the validation of the proposed framework is made to sections which are commonly assumed for visual grading of existing timber elements. Therefore, according to the shape and condition of the beam, six different sections were analyzed. They are distributed along the beam in areas where higher load level is expected and in section where geometry changes or high decay were observed (Figure 11.a). Due to the dimensions, four drillings are made in each analyzed section (two horizontal and two vertical drillings). All vertical drillings start at the bottom of the beam. The entry points of the drilling bit are known. However, due to the condition of the beam, it is not possible to see the exit point since the top face is in contact with the floor boards. In the horizontal drillings the entry and exit points are known. Tests were made with a 3450-S Resistograph from RINNTECH.

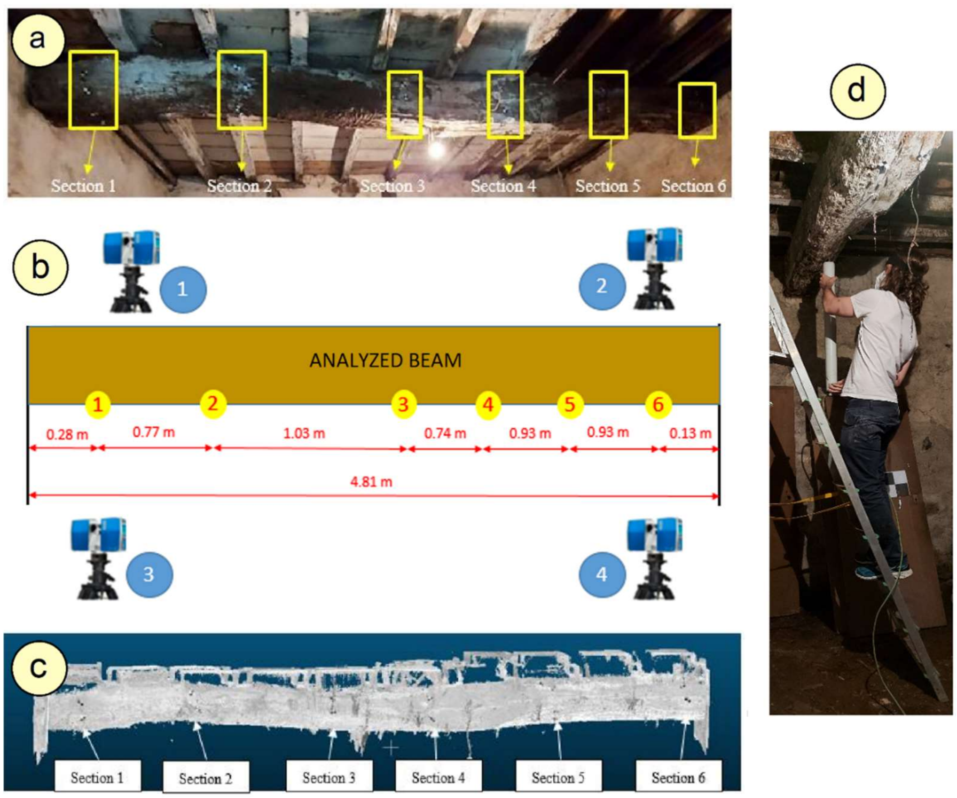

Figure 11. a) Photograph of the beam and all the analyzed sections, b) Detail drawing of the position of each section and the laser scan points, c) Point cloud of the beam.

During the test process, targets were placed in the entry and exit points of the drilling bit in the three visible faces of the beam. After the drilling resistance test, the beam was scanned from all four corners of the room with a FOCUS 3D X 130-HDR laser scan from FARO. Targets were previously placed along the walls in order to facilitate the later point cloud registration (Figure 11.b). Once all scans were registered in a single cloud point, a final cleaning was performed as to obtain the complete beam cloud point (Figure 11.c). On the basis of the point cloud, the different analyzed sections were obtained and the algorithm was applied in each of them. In this case, the open-face section closing function of the algorithm was also applied.

4.3. Results and discussion

Figure 12 shows the obtained results for each of the analyzed sections. The apparent perimeter has been drawn in blue; in green, the approximate resistant polygon; in black, the improved resistant section; and in red, the drillings. It must be noted that in the hidden face (the top face, Figure 12) the resistant and apparent area are coincident. This happens because the section closure is automatically performed by the algorithm.

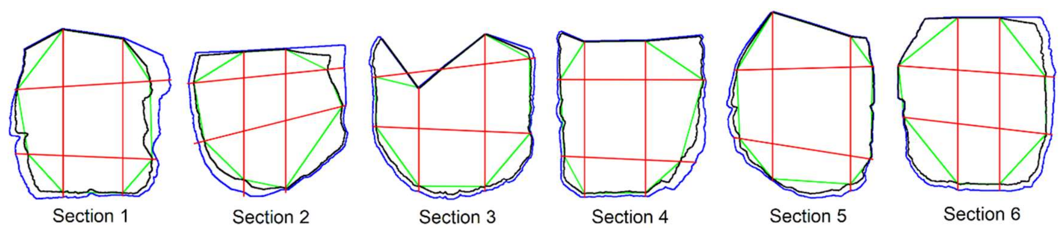

Figure 12. Results obtained in each of the studied beam sections.

Results of Section 3 require a more detailed explanation. Figure 13 presents the 3.1. drilling test graphs and proves how the found resistance decreases and increases again at the end. Due to the moment in which the resistance increases, it is possible to confirm that the drilling bit pierces the tables of the ceiling. Figure 13 also shows the 3.3. drilling test graph where, in the initial part of drilling 3, occurs a considerable fall in the resistance of the timber. It recovers after about 50 mm, confirming that in this area there is a large hole or crack in the beam. In the upper part this crack has a minor width as shown in the figure. However, it cannot be exactly measured due to the impossibility of accessing that face of the beam. Therefore, the resistant area of the beam will be larger than the calculated, being the calculation of the area and the resistant inertia moments on the conservative side for this specific case study.

The decay degree of the beam can be calculated from the apparent section, obtained by the cloud point, and the resistant section, obtained by the algorithm. The results are showed in Figure 14, where it is possible to observe that the most affected areas in all parameters are the first two sections. In fact, in section 1, decay has an area reduction of 15.2%; but also has inertia moments reduction in X (19.5%) and Y (35.5%). The four remaining sections show similar values. The most important decay effects in all the analyzed spans are produced in the vertical axis inertia moment. The average degradation has an area reduction effect of 10.3% and of inertia moments of 19.4%.

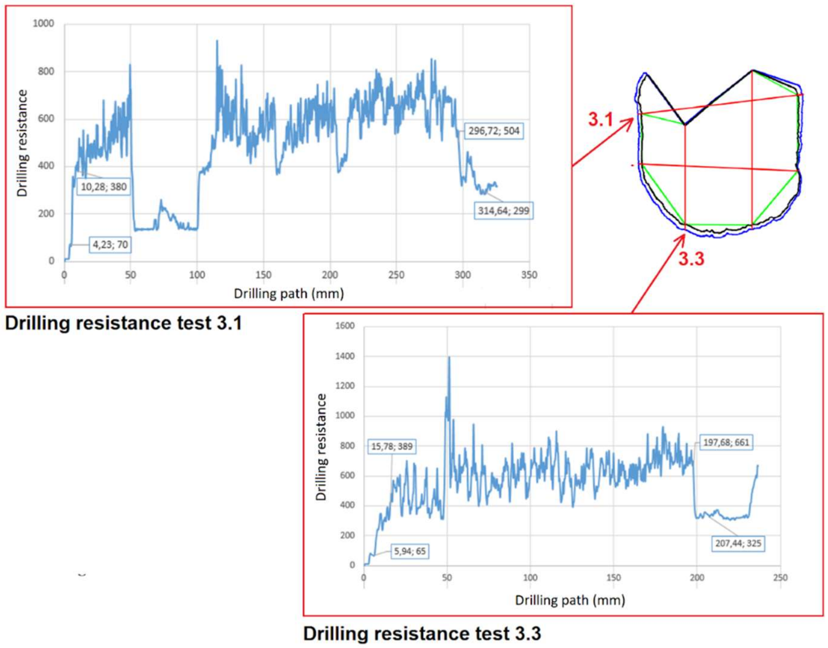

Figure 13. Detailed drilling resistance graph of section 3.

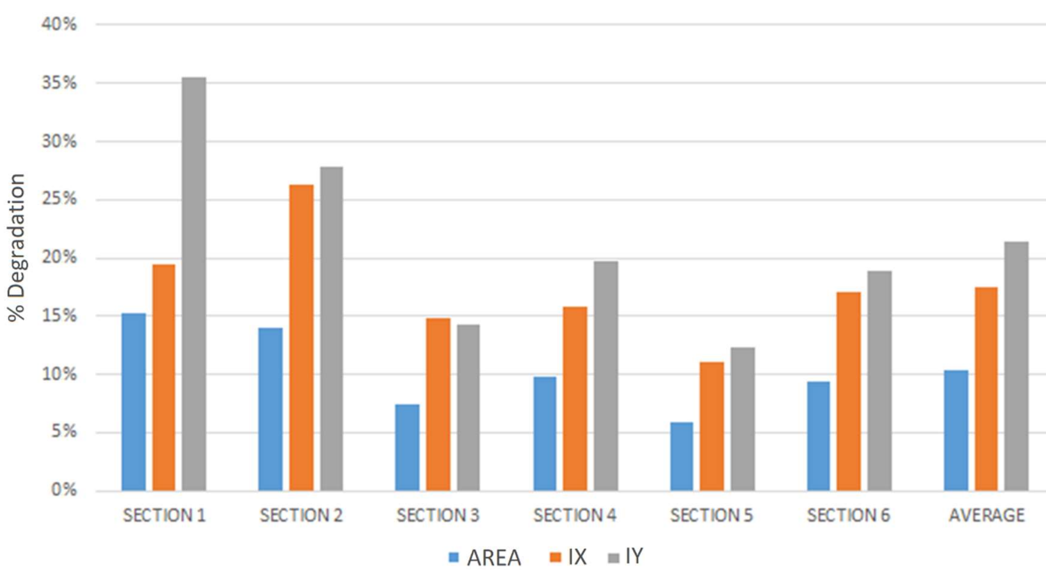

Figure 14. Area percentage and decayed inertia moments.

Since the beam belongs to an existing building, it is not possible to slice it and establish the apparent and resistant real values to compare them. Therefore, the resistant polygon (octagon, in this case) area calculated by traditional methods will be compared to the results obtained by the developed algorithm. Figure 15 shows how the average improvement achieved by the algorithm regarding current methods (polygonal resistant area) exceeds 12.4% in area and 23.9% in inertia moments, without considerable variations between the different areas. These results confirm that the algorithm corrections are significant.

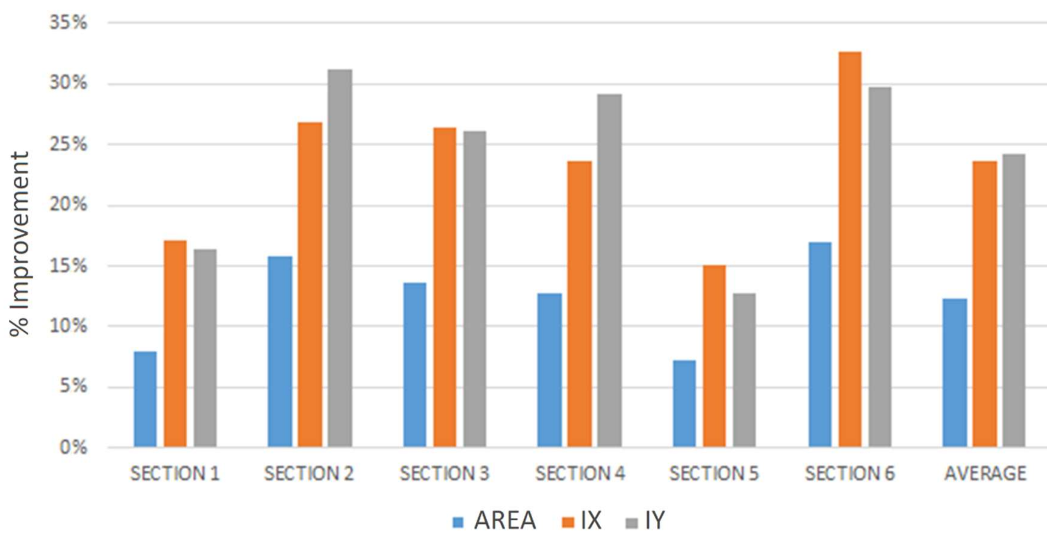

Figure 15. Improvement achieved by the algorithm in the resistant section calculation regarding to traditional methods (polygonal section).

4.4. Structural analysis of the beam

For a more complete and structural analysis of the beam belonging to the building hall, which is the purpose on structural health analysis of historic buildings, a 3D modeling of the beam was initiated by employing the resistant sections calculated by the algorithm. This analysis is made to validate the algorithm from a section scale to the element scale. Comparison is made between the element considering the polygonal residual cross-section by using or not the proposed framework.

Starting from the longitudinal position of each analyzed and calculated section, a progressive extrusion 3D model was created (Figure 16). The extrusion between analyzed sections is made assuming a linear variation of geometry. This is only possible due to the initial assumptions to select the sections to analyze where significant geometry change was a criterion for the section selection.

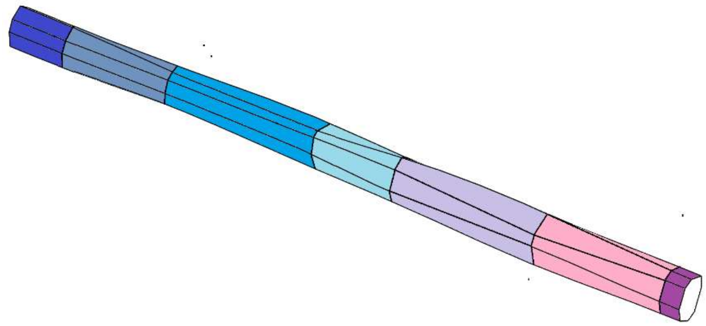

Figure 16. Progressive extrusion of the beam following the form of each analyzed section.

Following the same process, the beam was modelled with the octagonal resistant section in order to see the differences in the deformation calculation of both beams. For the calculation, the beam was assumed to have both fixed ends and a uniformly distributed vertical load with the same intensity in both cases (Figure 17). The timber element was identified as hardwood and visually graded according to UNI 11119 standard [27]. According to that visual grading the following properties were considered in the structural model: compression parallel to grain of 9 N/mm^2, bending strength of 10 N/mm^2, tension parallel to the grain of 9 N/mm^2, shear stress parallel to grain of 0.7 N/mm^2 and bending modulus of elasticity of 9000 N/mm^2.

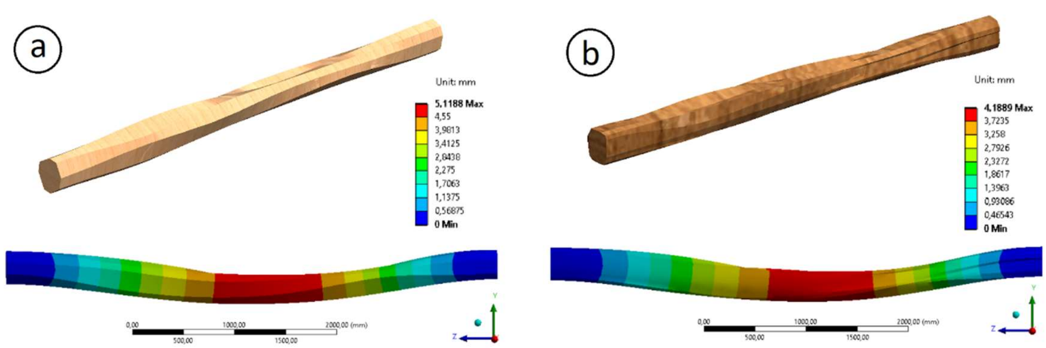

Figure 17. Deformation calculation of the case study beam. a) With the polygonal resistant section, b) With the improved resistant section.

Results show that, for the same load, deformation was 5.1 mm in the case of the beam with octagons, while in the beam made with sections obtained by the algorithm deformation was 4.2 mm. Hence, by employing the obtained section by the algorithm, deformation is, in this case, 22% lower, which is aligned with the results obtained for the average improvement in the calculation of the inertia moments.

5. CONCLUSION

This work allowed to develop an algorithm that, based on the data obtained by laser scanning and drilling resistance tests, obtains a more accurate geometry of the resistant cross-section of existing timber beams. The proposed algorithm improved the accuracy of measurement of area and inertia of the residual cross-section when comparing to the current methods using only the polygon obtained by drilling resistance test. In the experimental campaign, average error values lower than 3% and 7% are found for the area and inertia respectively, using the proposed algorithm, whereas traditional methods may arrive up to average errors of approximately 9% for area and 20% for inertia if two drillings measurements are made per direction.

Besides, the new algorithm allows to maintain a more uniform error on the definition of area and inertia, independently of the number of drillings. The average error for area found when considering different combinations on the number of drilling resistance tests per surface is approximately 2.4% with a standard deviation of 0.2%. With these values, it was possible to validate the algorithm within laboratory testing conditions, especially with two drillings (one of the most common methods), where the progress made regarding results of only using drilling resistance tests is significant. The average error committed by the algorithm in the two-drilled resistant area calculation is lower than the one committed by current calculation methods of six-drilled polygonal resistant area. In this case the error of the proposed algorithm is only 2.2% for just two measurements (one measurement per face), whereas traditional methods may rise up to 9% even considering twice the number of drilling resistance tests (two measurements per face).

By means of the progressive extrusion, based on the optimized resistant sections, 3D models of the beams can be obtained. The level of accuracy is directly related to decrease in the error obtained from the definition of the individual cross-sections. Furthermore, the developed algorithm enables the optimized calculation of the resistant section for those in which one of the faces cannot be seen or scanned.

In conclusion, the developed algorithm represents an advance in the analysis of decayed timber structures. It may improve the results obtained by the previous methods employed in the study of resistant sections in timber beams with signs of decay, even considering a reduction of the number of measurements. It allows to minimize the error in the definition of area and inertia of the resistant sections, and consequently may avoid valid beams to be dismissed due to regulation fulfillment from a resistance point of view, using more precise calculation methods. It must be noted that the algorithm provides a more accurate determination of the resistant cross-section which can either be more or less conservative than the traditional methods, as this is case study dependent. In that scenario, more extensive parametric studies regarding different dispositions of apparent and residual cross-sections must be studied, especially when having different levels of decay within the same element.

ACKNOWLEDGEMENTS

This work has been supported by the Spanish Ministry of Science and Innovation through the LASTING project (grant RTI2018-095893-B-C21) and SIRMA project, which is co-financed by the INTERREG Atlantic Area Programme through the European Regional Development Fund (ERDF) with application code: EAPA_826/2018. Also, acknowledge to the University of Minho for the stay made by Manuel Cabaleiro (35563149C) in the academic year 2020-2021. This work was partly financed by FCT / MCTES through national funds (PIDDAC) under the R&D Unit Institute for Sustainability and Innovation in Structural Engineering (ISISE), under reference UIDB / 04029/2020.

6. REFERENCES

[1] L. Sanhudo, N.M. Ramos, J.P. Martins, R.M. Almeida, E. Barreira, M.L. Simoes, V. Cardoso, A framework for in-situ geometric data acquisition using laser scanning for BIM modelling, Journal of Building Engineering 28 (2020) 101073, https://doi.org/10.1016/j.jobe.2019.101073.

[2] F.M. Dinis, L. Sanhudo, J.P. Martins, N.M. Ramos, Improving project communication in the architecture, engineering and construction industry: coupling virtual reality and laser scanning, Journal of Building Engineering 30 (2020) 101287, https://doi.org/10.1016/j.jobe.2020.101287.

[3] H.A. Jaafar, X. Meng, A. Sowter, P. Bryan, New approach for monitoring historic and heritage buildings: using terrestrial laser scanning and generalised Procrustes analysis, Struct. Contr. Health Monit. 24 (11) (2017), e1987, https://doi.org/10.1002/stc.1987.

[4] M. Cabaleiro, B. Riveiro, B. Conde, A. Sanchez.. A case study of measurements of deformations due to different loads in pieces less than 1 meter from lidar data. Measurement, , (2020) 107196 1-10p. https://doi.org/10.1016/j.measurement.2019.107196

[5] Á. Bautista-De Castro, L.J. Sánchez-Aparicio, L.F. Ramos, J. Sena-Cruz, D. González-Aguilera, Integrating geomatic approaches, Operational Modal Analysis, advanced numerical and updating methods to evaluate the current safety conditions of the historical Bôco Bridge, Construct. Build. Mater. 158(2018) 961–984. https://doi.org/10.1016/j.conbuildmat.2017.10.084

[6] L.J. Sánchez-Aparicio, S. Del Pozo, L.F. Ramos, A. Arce, F.M. Fernandes, Heritage site preservation with combined radiometric and geometric analysis of TLS data, Automat. Construct. 85 (2018) 24–39. https://doi.org/10.1016/j.autcon.2017.09.023

[7] M. Chen, E. Koc, Z. Shi, L. Soibelman, Proactive 2D model-based scan planning for existing buildings, Automat. Construct. 93 (2018) 165–177. https://doi.org /10.1016/j.autcon.2018.05.010

[8] M. Cabaleiro, B. Riveiro, P. Arias, J.C. Caamaño, Algorithm for the analysis of the geometric properties of cross-sections of timber beams with lack of material from LIDAR data. Materials and Structures, 10(49), (2016) 4265-4278.https://doi.org/10.1617/s11527-015-0786-0

[9] L. Fregonese, L. Taffurelli, 3D model for the documentation of cultural heritage: the wooden domes of St. Mark's Basilica in Venice, the International Archives of the Photogrammetry, Remote Sensing and Spatial Information Sciences 38 (Part 5) (2009) W1.

[10] M. Cabaleiro, J.M. Branco, H.S. Sousa, B. Conde, First results on the combination of laser scanner and drilling resistance tests for the assessment of the geometrical condition of irregular cross-sections of timber beams, Materials and Structures. 51 (4) (2018) 99, https://doi.org/10.1617/s11527-018-1225-9

[11] H. Edelsbrunner, E.P. Mücke, Three-dimensional Alpha Shapes, ACM Trans.Graphics 13 (1) (1994) 43–72.

[12] G. Y. Jeong, T. N. Nguyen, D. K. Tran, T. B. H. Hoang, Applying unmanned aerial vehicle photogrammetry for measuring dimension of structural elements in traditional timber building. Measurement, 153 (2020) 107386. https://doi.org/10.1016/j.measurement.2019.107386

[13] S. Casans, T. Iakymchuk, A. Rosado-Muñoz. High resistance measurement circuit for fiber materials: Application to moisture content estimation. Measurement, 119 (2018) 167-174. https://doi.org/10.1016/j.measurement.2018.01.072

[14] A. Ettelaei, M. Layeghi, H. Z. Hosseinabadi, G. Ebrahimi, Prediction of modulus of elasticity of poplar wood using ultrasonic technique by applying empirical correction factors. Measurement, 135 (2019) 392-399. https://doi.org/10.1016/j.measurement.2018.11.076

[15] Y. Yu, Y. Liu, M. Gong, Z. Xu, Y. Fang, R&R study of using a stress wave timer to measure the elastic modulus of structural dimension lumber. Measurement, 95 (2017) 293-296. https://doi.org/10.1016/j.measurement.2016.10.040

[16] A. C. Altunisik, , E. R. O. L. Kalkan, F. Y. Okur, K. Ozgan, O. Ş. Karahasan, A. Bostanci, Non-destructive modal parameter identification of historical timber bridges using ambient vibration tests after restoration. Measurement, 146 (2019) 411-424. https://doi.org/10.1016/j.measurement.2019.06.051

[17] J. M. Branco, H. S. Sousa, E. Tsakanika, Non-destructive assessment, full-scale load-carrying tests and local interventions on two historic timber collar roof trusses. Engineering Structures, 140 (2017) 209-224. https://doi.org/10.1016/j.engstruct.2017.02.053

[18] T.P. Nowak, J. Jasie´nko, K. Hamrol-Bielecka, In situ assessment of structural timber using the resistance drilling method–Evaluation of usefulness, Construct.Build. Mater. 102 (2016) 403–415, https://doi.org/10.1016/j.conbuildmat.2015.11.004.

[19] T. Tannert, R.W. Anthony, B. Kasal, M. Kloiber, M. Piazza, M. Riggio, N. Yamaguchi, In situ assessment of structural timber using semi-destructive techniques, Mater. Struct. 47 (5) (2014) 767–785, https://doi.org/10.1617/s11527-013-0094-5.

[20] T. Lechner, T. Nowak, R. Kliger, In situ assessment of the timber floor structure of the Skansen Lejonet fortification, Sweden, Construct. Build. Mater. 58 (2014) 85–93, https://doi.org/10.1016/j.conbuildmat.2013.12.080.

[21] C. Liao, H. Zhang, X. Wang, D. Li, Condition assessment of wood structural members at yu tomb of the ming dynasty, China, Materials and Structures 48 (10) (2015) 3259–3267, https://doi.org/10.1617/s11527-014-0396-2.

[22] J.M. Branco, H.S. Sousa, E. Tsakanika, Non-destructive assessment, full-scale loadcarrying tests and local interventions on two historic timber collar roof trusses, Eng. Struct. 140 (2017) 209–224, https://doi.org/10.1016/j.engstruct.2017.02.053.

[23] B. Becerik-Gerber, F. Jazizadeh, G. Kavulya, G. Calis, Assessment of target types and layouts in 3D laser scanning for registration accuracy, Autom. Constr. 20 (5) (2011) 649–658. https://doi.org/10.1016/j.autcon.2010.12.008

[24] L. Leng, T. Zhang, L. Kleinman, W. Zhu, Ordinary least square regression, orthogonal regression, geometric mean regression and their applications in aerosol science. J. Phys. Conf. Ser., 78 (2007) 012084.

[25] R. Maronna, Principal components and orthogonal regression based on robust scales. Technometrics, 47 (2005) 264–273. https://doi.org/10.1198/004017005000000166

[26] M.Cabaleiro, J. Hermida, B. Riveiro, J. C. Caamaño, Automated processing of dense points clouds to automatically determine deformations in highly irregular timber structures. Construction and Building Materials, 146 (2017) 393-402. https://doi.org/10.1016/j.conbuildmat.2017.04.037

[27] UNI. UNI 11119. Cultural heritage – wooden artifacts – load-bearing structures – on site inspections for the diagnosis of timber members. Milano: Ente Nazionale Italiano di Unificazione (2004)-